COMBINING TOOL WEAR AND STABILITY IN HIGH-SPEED MACHINING PERFORMANCE PREDICTION

Jaydeep M. Karandikar, Raúl E. Zapata, and Tony L. Schmitz
Department of Mechanical and Aerospace Engineering
University of Florida
Gainesville, FL, USA

INTRODUCTION

Tool wear imposes an important process limitation in milling, along with chatter (self-excited vibrations) and surface location error (due to forced vibrations). Prior research has shown an increase in the cutting forces and, subsequently the force model coefficients, as a result of tool wear [1]. Therefore, tool wear effects can be incorporated through the force model coefficients used to calculate stability lobe diagrams, which graphically represent the boundary between stable and unstable combinations of spindle speed and axial depth of cut. This research explores tool wear as a process limitation through its effect on milling stability lobes.

This is achieved using the milling "super diagram" that incorporates limitations to milling productivity and part quality imposed by stability, surface location error, and tool wear [2]. Combinations of axial depth of cut and spindle speed that offer stable cutting conditions with an acceptable, user-defined surface location error (SLE) level are identified using a gray-scale color coding scheme. The effect of tool wear is incorporated by determining the variations in force model coefficients used for process dynamics prediction with tool wear. The force model coefficients tend to increase as a function of the flank wear width (used as a measure of tool wear). The increase in force model coefficients is determined as a function of the volume of material removed. Using these coefficients, a unique super diagram is constructed for any user-defined volume of material removed using the selected cutter. Additionally, user beliefs about data and model accuracy are applied to identify safety margins relative to the deterministic boundaries in the diagrams.

In this paper, experimental results are provided for an inserted (carbide) cutter used to machine 1018 steel. The wear behavior is incorporated as changes in the force model coefficients as a function of the volume of material removed at different operating parameters. The flank wear is also measured using an on-machine microscope (to avoid tool removal from the spindle) and correlated to the force model coefficients. Super diagrams are developed that correspond to the new and worn tool performance and experimental results are provided to verify changes in the process stability with tool wear.

TOOL WEAR TESTS

In this section, the experimental steps required to collect the tool wear data for the new super diagram are described for a 19 mm diameter inserted endmill (one square uncoated Kennametal 107888126 C9 JC carbide insert; zero rake and helix angles, 15 deg relief angle, 9.53 mm square x 3.18 mm) that was used to machine 1018 steel.

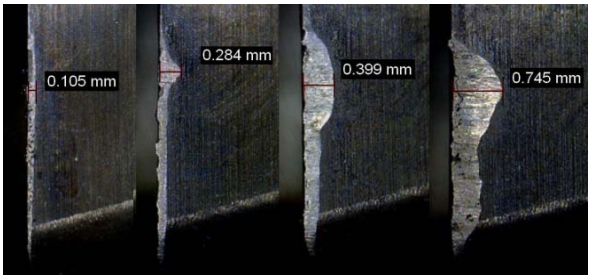

FIGURE 1. Images of FWW at 60x magnification (from left to right, V *= {50, 125, 200, and 275} cm^3).*

$$F_t = K_t bh + K_{te} b$$
$$F_n = K_n bh + K_{ne} b \quad (1)$$

The cutting forces were monitored using a table-mounted force dynamometer (Kistler 9257B) and the four cutting force coefficients in Eq. 1 were identified intermittently while wearing the tool by performing a linear regression to the mean x (feed) and y direction forces over a range of feed per tooth values: {0.03, 0.04, 0.05, 0.06, and 0.07} mm/tooth [3,4]. The feed per tooth while wearing the tool was kept constant at 0.06 mm/tooth. The radial and axial depths of

cut were 4.7 mm (25% radial immersion) and 3 mm.

In addition to monitoring the cutting force, the insert wear status was also measured at intervals of volume of material removed, V. To avoid removing the insert/tool from the spindle, a handheld microscope (60x magnification) was used to record the rake and flank surfaces. The calibrated digital images were used to identify the FWW (no crater wear was observed). Example results for a spindle speed, Ω, of 2500 rpm are provided in Fig. 1.

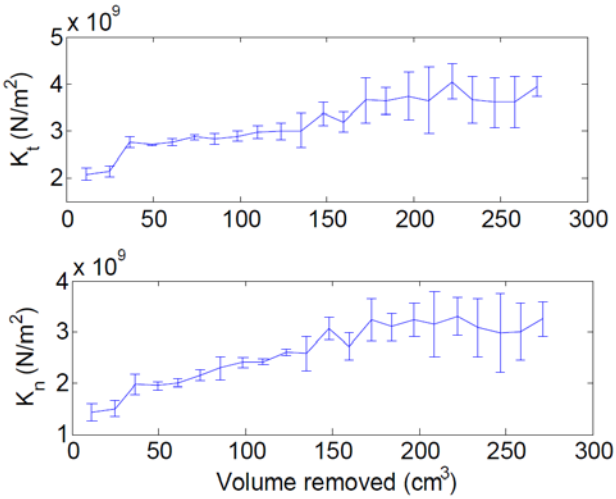

FIGURE 2. Variation in K_t and K_n with volume removed (Ω = 2500 rpm).

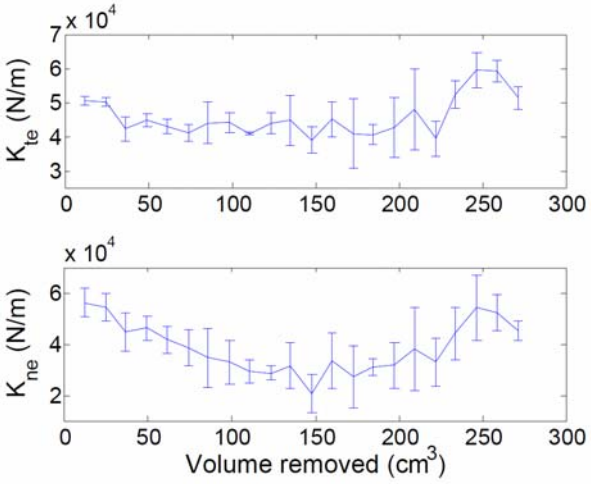

FIGURE 3. Variation in K_{te} and K_{ne} with volume removed (Ω = 2500 rpm).

At V intervals of 12 cm^3, the four cutting force coefficients were determined. These results are given in Figs. 2 and 3. For the tool/material pair tested here, there was an approximately linear growth in K_t and K_n, while the K_{te} and K_{ne} values showed no clear trend.

To evaluate the change in coefficient behavior with spindle speed, additional tests were completed at {3750, 5000, 6250, and 7500} rpm. The results are displayed in Fig. 4, as well as the linear least squares fits. As expected, the rates of K_t and K_n growth (i.e., the slopes) increase with spindle speed. While the results are not shown, the K_{te} and K_{ne} values again did not exhibit any significant trend at the additional spindle speeds.

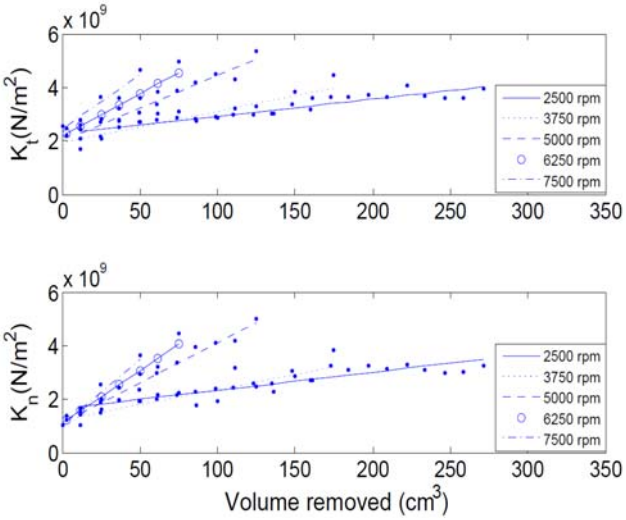

FIGURE 4. Variation in K_t and K_n with volume removed for various spindle speeds.

The slopes of the individual (K_t and K_n versus volume removed) lines in Fig. 4 are plotted against spindle speed in Fig. 5. It is seen that these slopes grow linearly with increasing speed. Therefore, a model which linearly relates the K_t and K_n values to Ω and V can be applied for this tool-material pair; see Eq. 3. The slopes of the lines in Fig. 5 are 7.1×10^3 $(N/m^2/cm^3)$/rpm for the K_t data and 9.1×10^3 $(N/m^2/cm^3)$/rpm for the K_n data. The intercepts for the linear relationships in Eq. 3 are determined from the mean V = 0 (new tool) values from Fig. 2. Because a significant trend in K_{te} and K_{ne} was not observed, these values can be set equal to the mean values from Fig. 3, i.e., $K_{te} = 4.6\times10^4$ N/m and $K_{ne} = 3.9\times10^4$ N/m. Given this relationship, the super diagram that incorporates tool wear can then be developed by applying the

user-selected volume and calculating K_t and K_n for each spindle speed in the {Ω, b} domain.

$$K_t(\Omega,V) = 2.2\times10^9 + (7.1\times10^3\cdot\Omega)V$$
$$K_n(\Omega,V) = 1.2\times10^9 + (9.1\times10^3\cdot\Omega)V \quad (2)$$

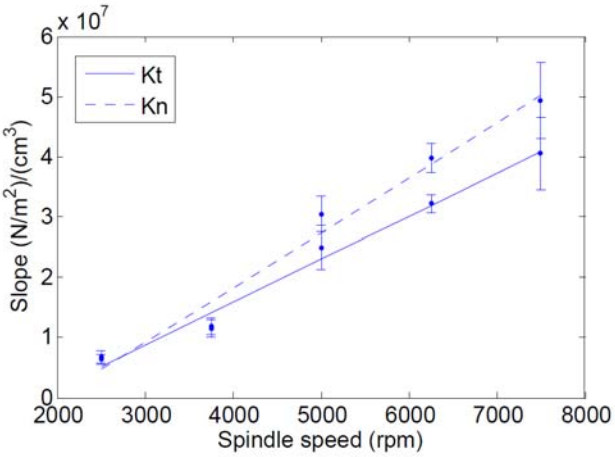

FIGURE 5. Variation in slope of K_t and K_n versus volume removed lines (from Fig. 4) with spindle speed.

STABILITY TESTS

The tool wear experimental results showed a linear increase in cutting force coefficients K_t and K_n with volume removed due to progressive flank wear. The rate of increase of force coefficients increased linearly with speed. This increase in force coefficients causes the limiting axial depth of cut to decrease. To explore this wear effect, the tool point frequency response function was measured by impact testing and the stability limit was calculated using force coefficients based on a new and worn insert. An insert was worn by removing 275 cm^3 at Ω = 2500 rpm. The force coefficients were determined for both a new insert and the worn insert using a linear regression of the average x and y direction forces at varying feed per tooth values as described previously. These force coefficients are provided in Table 1. For stability testing at 5100 rpm, the equivalent volume removed which would yield the K_t and K_n values for the worn insert was calculated to be 121 cm^3 using Eq. 2. The stability limit for the new insert was calculated using the new insert values (V = 0). For the worn insert, the K_t and K_n values at each spindle speed were calculated using Eq. 2 and the stability limit was generated [5]. However, as shown by the error bars in Fig. 5, there is uncertainty in the K_t and K_n values for both the new and worn inserts. A Monte Carlo simulation was completed where random K_t and K_n values were selected from the experimental distributions and a new stability limit was calculated for each set. See Fig. 6, where the radial depth of cut is equal to the tool diameter (slotting). The band of stability limits indicates the uncertainty. This information could be used, for example, to aid a user in selecting his/her safety limits for the super diagram. The mean limiting depth of cut at 5100 rpm is 2.15 mm for the new insert and 0.85 mm for the worn insert.

Table 1: Force coefficient values for new and worn inserts.

	K_t (N/m^2)	K_n (N/m^2)	K_{te} (N/m)	K_{ne} (N/m)
New	1.90×10^9	0.78×10^9	45500	46650
Worn	4.98×10^9	4.51×10^9	45500	25500

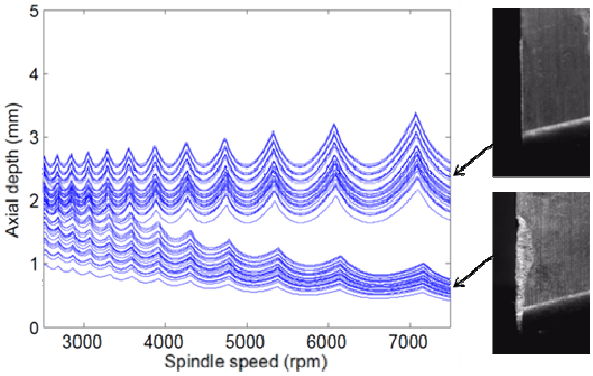

FIGURE 6. Stability lobe diagram for new (V = 0) and worn inserts (V = 121 cm^3).

Cutting tests were completed at b = {0.8, 1.6, 2.2, and 3} mm with the new and worn inserts. A once-per-revolution force sampling strategy for the x (F_x) and y (F_y) directions was used to identify chatter. The once-per-revolution samples were obtained by sampling the force data at the commanded spindle rotating frequency. For stable cutting conditions, the once-per-revolution samples (due to forced vibration only) are synchronous with spindle rotation and produce a small cluster of points [6] in the F_x vs. F_y plot. Unstable behavior, on the other hand, produces a more distributed set of points due to its asynchronous nature. A statistical variance ratio, R, is used as an indicator of chatter [7]; see Eq. 3, where $\sigma^2_{opr,x}$ and $\sigma^2_{opr,y}$ are the variances in the once-per-revolution sampled forces in the x and y directions and σ^2_x and σ^2_y are the variances in the x and y direction forces. Figure 7 shows

once-per-revolution samples for tests at b = 1.6 mm and Ω = 5100 rpm for the new and worn inserts.

$$R = \frac{\sigma^2_{opr,x} + \sigma^2_{opr,y}}{\sigma^2_x + \sigma^2_y} \quad (3)$$

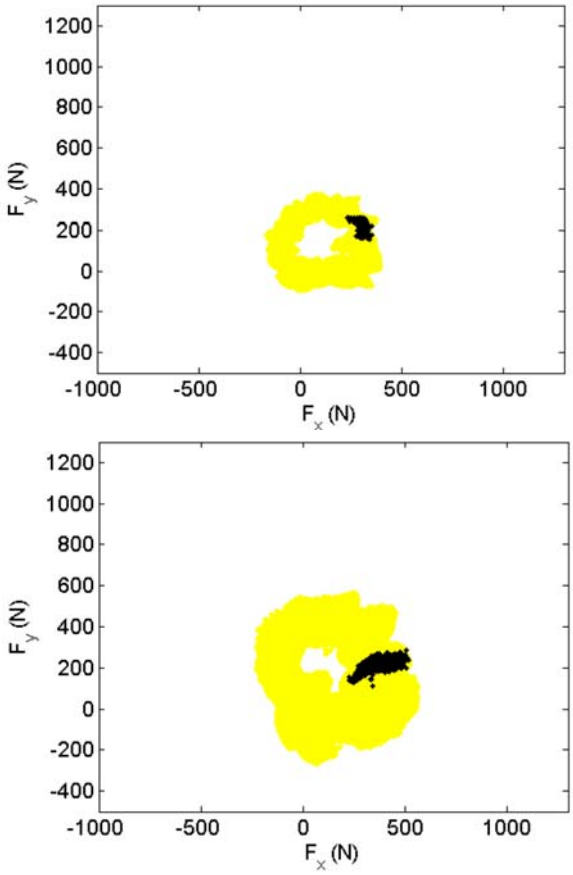

FIGURE 7. Once-per-revolution samples for 1.6 mm axial depth of cut and 5100 rpm spindle speed (top: new insert, bottom, worn insert).

As seen in Fig. 7, the distribution of once-per-revolution samples increases for the unstable cut using the worn insert. Similar results were obtained b = 0.8 mm (which is within the stability limit distribution for the worn tool in Fig. 6), 2.2 mm, and 3 mm. Figure 8 shows the R values for different axial depths of cut, where the R value is larger for all cuts with the worn insert and increases substantially for both the new and worn insert at b = 3 mm (violent chatter occurred in both cases for this depth).

CONCLUSIONS

In this work, the effect of tool wear on milling stability was evaluated experimentally. By modifying the force model coefficients according to the wear status (as a function of volume removed), tool wear effects were incorporated into the milling super diagram. Cutting tests were completed to verify the change in process stability with tool wear status.

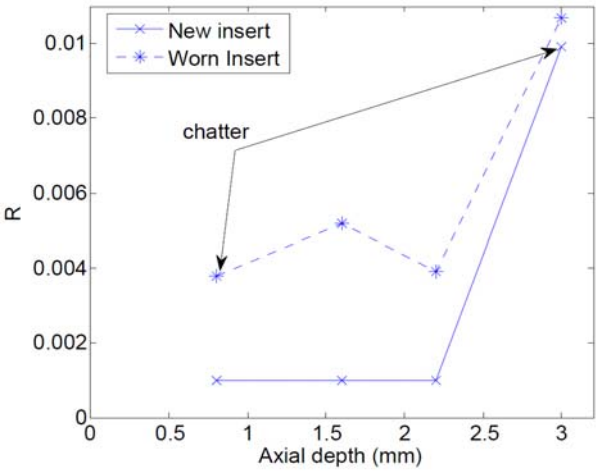

FIGURE 8. Variance ratio, R*, for new and worn inserts at different axial depths of cut.*

REFERENCES

[1] Cui, Y., B. Fussell, R., Jerard, and D. Esterling (2009). Tool Wear Monitoring for Milling by Tracking Cutting Force Model Coefficients. Transactions of the NAMRI/SME, Vol. 37, pp. 613-620.

[2] Zapata, R., J. Karandikar, and T. Schmitz, (2009). A New 'Super Diagram' for Describing Milling Dynamics. Transactions of NAMRI/SME, Vol. 37, pp. 245-252.

[3] Altintas, Y. (2000). Manufacturing Automation. Cambridge University Press, Cambridge, UK.

[4] Schmitz, T. and K.S. Smith (2009). Machining Dynamics: Frequency Response to Improved Productivity, Springer, NY.

[5] Altintas, Y. and E. Budak (1995). Analytical Prediction of Stability Lobes in Milling. Annals of the CIRP, Vol. 44/1, pp. 357-362.

[6] Davies M., B. Dutterer, J. Pratt, A. Schaut, and J. Bryan (1998). On the Dynamics of High-Speed Milling with Long, Slender Endmills, Annals of the CIRP, Vol. 47/1, pp. 55-60.

[7] Cheng C., T. Schmitz T., and G.S. Duncan (2007). Rotating Tool Point Frequency Response Prediction using RCSA, Machining Science and Technology, 11, pp. 433-446.